Hot embossing of Au- and Pb-based alloys for x-ray grating fabrication

Romano, Lucia ; Vila-Comamala, Joan ; Schift, Helmut ; Stampanoni, Marco ; Jefimovs, Konstantins

Abstract: Grating-based X-ray phase-contrast interferometry has a high application impact in materials science and medicine for imaging of weakly absorbing (low Z) materials and soft tissues. For absorbing gratings, casting of highly X-ray absorbing metals, such as Au and Pb alloys, has proven to be a viable way to generate large area periodic high aspect ratio microstructures. In this paper, the authors review the grating fabrication strategy with a special focus on a novel approach of casting low temperature melting alloys (Au-Sn and Pb-based alloys) into Si grating templates using hot embossing. This process, similar to nanoimprint lithography, requires particular adjusting efforts of process parameters as a function of the metal alloy and the grating feature size. The transition between the solid and liquid state depends on the alloy phase diagram, the applied pressure can damage the high aspect ratio Si lamellas, and the microstructure of the solid metal can affect the grating structure. The authors demonstrate that metal casting by hot embossing can be used to fabricate gratings on a large area (up to 70 × 70 mm2) with an aspect ratio of up to 50:1 and a pitch in the range of 1–20 m.

DOI: https://doi.org/10.1116/1.4991807

Hot embossing of Au- and Pb-based alloys for x-ray grating fabrication

Lucia Romano, Joan Vila-Comamala, Helmut Schift, Marco Stampanoni, and Konstantins Jefimovs

Citation: Journal of Vacuum Science & Technology B, Nanotechnology and Microelectronics: Materials, Processing, Measurement, and Phenomena **35**, 06G302 (2017); doi: 10.1116/1.4991807

View online: https://doi.org/10.1116/1.4991807

View Table of Contents: http://avs.scitation.org/toc/jvb/35/6

Published by the American Vacuum Society

Hot embossing of Au- and Pb-based alloys for x-ray grating fabrication

Lucia Romano[a)]
Paul Scherrer Institut, 5232 Villigen PSI, Switzerland; Institute for Biomedical Engineering, University and ETH Zürich, 8092 Zürich, Switzerland; and Department of Physics and CNR-IMM, University of Catania, 64 via S. Sofia, Catania I-95123, Italy

Joan Vila-Comamala
Paul Scherrer Institut, 5232 Villigen PSI, Switzerland and Institute for Biomedical Engineering, University and ETH Zürich, 8092 Zürich, Switzerland

Helmut Schift
Paul Scherrer Institut, 5232 Villigen PSI, Switzerland

Marco Stampanoni and Konstantins Jefimovs
Paul Scherrer Institut, 5232 Villigen PSI, Switzerland and Institute for Biomedical Engineering, University and ETH Zürich, 8092 Zürich, Switzerland

(Received 23 June 2017; accepted 24 August 2017; published 8 September 2017)

Grating-based X-ray phase-contrast interferometry has a high application impact in materials science and medicine for imaging of weakly absorbing (low Z) materials and soft tissues. For absorbing gratings, casting of highly X-ray absorbing metals, such as Au and Pb alloys, has proven to be a viable way to generate large area periodic high aspect ratio microstructures. In this paper, the authors review the grating fabrication strategy with a special focus on a novel approach of casting low temperature melting alloys (Au-Sn and Pb-based alloys) into Si grating templates using hot embossing. This process, similar to nanoimprint lithography, requires particular adjusting efforts of process parameters as a function of the metal alloy and the grating feature size. The transition between the solid and liquid state depends on the alloy phase diagram, the applied pressure can damage the high aspect ratio Si lamellas, and the microstructure of the solid metal can affect the grating structure. The authors demonstrate that metal casting by hot embossing can be used to fabricate gratings on a large area (up to $70 \times 70\,\mathrm{mm}^2$) with an aspect ratio of up to 50:1 and a pitch in the range of 1–20 μm. © *2017 American Vacuum Society*. [http://dx.doi.org/10.1116/1.4991807]

I. INTRODUCTION

Grating-based X-ray phase-contrast interferometry (GI) enables phase contrast imaging with a much higher image contrast of weakly absorbing materials (such as soft tissues) than conventional absorption-based X-ray radiography imaging[1] with a relevant impact in material science and medical applications. The main challenge is the fabrication of the absorption gratings,[2] which are metal periodic microstructures with high aspect ratio. Micrograting with (1) high aspect ratio (in the range of 100:1, structural width in the micrometer range), (2) large area (mammography, e.g., requires for a field of view of $200 \times 200\,\mathrm{mm}^2$), and (3) good uniformity (no distortions and change in the period and height over the whole grating area) are required. Absorption gratings are usually fabricated by metal electroplating (typically of Au, which is one of the most efficient absorbing materials for X-rays) into high aspect ratio grating templates produced by deep X-ray lithography (also called LIGA)[3] or deep Si etching.[2] Microcasting for X-ray absorption gratings has been developed by using molten Bi (melting temperature, 271 °C) via capillary action and surface tension.[4–6] However, the low density (9.78 g/cm^3, atomic number 83) of Bi requires much higher (factor of 1.7 at 30 keV) aspect ratio structures to get an absorption comparable to that of Au (density 19.32 g/cm^3, atomic number 79). In a previous paper,[7] we demonstrated that metal microstructured optical elements for GI can be fabricated by using an alternative approach of Au-Sn microcasting into Si templates, which has the advantage of fast processing with a competitive cost and X-ray absorption only 20% less than pure Au (at an X-ray energy of 30 keV, see Table I). Metal casting can potentially be realized with any metal whose melting temperature is compatible with the available hot embossing tool and grating substrates. However, apart from cost issues and availability of suitable alloys for specific applications, differences are expected in terms of melting behavior, wetting, and morphology. In this work, we therefore extended the experiments to Pb (density 11.34 g/cm^3, atomic number 82)-rich compounds in comparison to Au-Sn alloys and we investigated the limits of the process in terms of grating stability, aspect ratio, and uniformity. We analyzed in detail the material properties as a function of the casting process in Si gratings for both classes of alloys: Au-Sn and Pb-based alloys. Three main material properties turned out to be relevant for the realization of metal gratings by hot embossing: (1) wettability of the grating surface with respect to the liquid metal used for casting; (2) phase diagram of the metal alloy in order to properly set up the temperature range and process conditions; (3) thermal stress and fracture behavior due to the mismatch in thermal expansion coefficients between the poly-crystalline metal and the crystalline Si. The three aspects are presented and

a)Electronic mail: lucia.romano@psi.ch

TABLE I. Summarizing the main metal properties and comparison of processing. The attenuation length is the depth into the material measured along the surface normal where the intensity of x-rays falls to 1/e of its value at the surface. It was calculated using Ref. 15. It is assumed that Au electroplating produces pure Au filling of the grating structures, which means with the same density of bulk Au.

Metal/alloy	Au electroplating	Au-Sn casting	Pb-In casting	Pb-Sn-Ag casting
Composition (wt. %)	Pure Au	80 wt. % Au 20 wt. % Sn Eutectic	95 wt. % Pb 5 wt. % In	92.5 wt. % Pb 5 wt. % Sn 2.5 wt. % Ag
Composition (at. %)	Pure Au	71 at. % Au 29 at. % Sn	91.3 at. % Pb 8.7 at. %In	87.2 at. % Pb 8.2 at. % Sn 4.6 at. % Ag
T (°C)		*Melting* 280	*Solidus* 292 *Liquidus* 314	*Solidus* 287 *Liquidus* 296
Density (g/cm^3)	19.32 (bulk material)	14.32	11.06	11.02
Attenuation length (X-ray 30 keV) (μm)	19.98	24.29	30.98	30.81
Attenuation length (%)	100	121	155	154
Process	(1) Growth of gold within grooves from the conducting seed layer	(1) Heating to 280 °C and pressure; (2) slow cooling (to avoid thermal shock)	(1) Heating to 292 °C and low pressure(2) Heating to 314 °C and high pressure, and mold filling	(1) Heating to 287 °C and low pressure(2) Heating to 296 °C and high pressure and mold filling
Remarks	polymer instability issues; process time from several hours to several days	needs a wetting layer (Ir by ALD); casting process time 30 min–4 h	pressure can already be applied in stage 1; formation of the wetting layer in stage 1; casting process time 30 min–1 h	needs a wetting layer (Ir by ALD); pressure can already be applied in stage 1; formation of melt with microparticles in stage 1 (possible damage); casting process time 30 min–1 h
Aspect ratio (4.8 μm pitch)	91:1 (Ref. 3, with bridges)	40:1 (Ref. 7) 50:1 (with bridges)	30:1 50:1 (with bridges)	20:1

discussed with few examples that helped to generalize the required material properties and grating design for metal casting fabrication.

X-ray preliminary characterization has been performed in order to investigate the uniformity of the metal filling on the grating area and the quality of the casted gratings in the interferometric set-up.

II. EXPERIMENT

Metal micrograting were fabricated according to the work flow described in Fig. 1. The pattern was designed by photolithography on Si ⟨100⟩ substrates (diameter of 100 mm), silicon etching was performed by deep reactive ion etching (Bosch process)[8] or metal assisted chemical etching (MacEtch),[9,10] and the process details are reported in Refs. 8–10. The pitch of the grating was in the range of 1–20 μm, the duty cycle was 0.5, and the grating area was $70 \times 70\,mm^2$. A conformal layer of Ir (20–30 nm Ir on 10 nm Al_2O_3) was later deposited by Atomic Layer Deposition (ALD, Picosun R-200 Ad.) to improve the wettability of the Si template with respect to the liquid metal alloy.[7] Metal casting was performed using a Jenoptik HEX 03 hot embossing tool, in vacuum (pressure in the range of 100–500 Pa), by pressing a metal foil with the same size as the grating in contact with the grating surface at the melting temperature of the metal foil. A 1 mm thick sheet of silicone rubber (i.e., polydimethylsiloxane) was used as a cushion layer for pressure equilibration and to smoothen out any kind of unevenness, e.g., caused by substrate bow and warp or even dust particles. A polished Si chip with a thickness of 500 μm was used as a flat surface to apply the pressure on the metal foil. The pressure was varied from 1 to 12 MPa. The temperature was controlled with a precision of 2 °C. Further details of the casting process are reported elsewhere.[7] Test samples with the size of $20 \times 20\,mm^2$ were cut from the original wafer. The optimized process was realized on the full wafer with a grating area of $70 \times 70\,mm^2$ (see Fig. 1). We used metal foils of the eutectic Au–Sn (80 wt. % Au–20 wt. % Sn with a melting temperature of 280 °C) alloy from Ametek; Pb–In (95 wt. % Pb–5 wt. % In, *liquidus* point 314 °C, *solidus* 292 °C) and Pb–Sn–Ag (92.5 wt. % Pb–5 wt. % Sn–2.5 wt. %

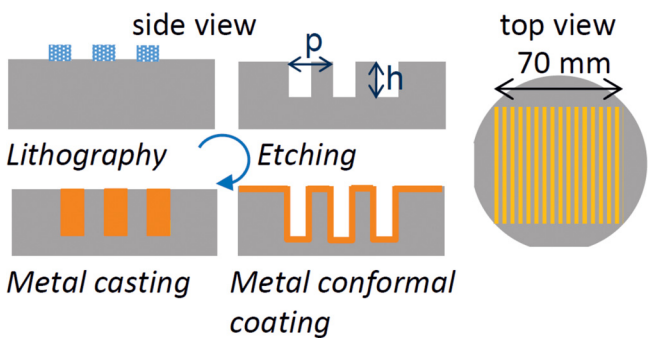

FIG. 1. (Color online) Schematic of the different stages of the fabrication sequence (not to scale): resist pattern by lithography, etched trenches, trenches/grooves with metal conformal coating, and completely filled trenches with zero excess material. The top view shows the grating area ($70 \times 70\,mm^2$) on a silicon wafer with a diameter of 100 mm.

Ag, *liquidus* point 296 °C, *solidus* 287 °C) compounds from Hi-Rel Alloys. For minimizing the excess of material, the thickness of the metal foil has to match the cavity volume of the grating. For Au-Sn foils, it is possible to choose the thickness in the range of 25–50 μm, while for Pb-based alloys, we used foils with a thickness of 100 μm since thinner foils are usually not commercially available in the size of $70 \times 70\,mm^2$.

A scanning electron microscope (SEM) Zeiss Supra VP55 was used to characterize the casted gratings in the cross-section. The X-ray performance of Au-Sn casted gratings with a pitch of 4.8 μm was investigated by setting up a laboratory X-ray grating interferometry system using a Hamamatsu L10101 X-ray microsource (35 kV voltage and 0.2 mA electron current) and a scintillator-fiber-optic coupled CCD X-ray detector (1024 × 1024 pixels of 13 μm).

III. RESULTS AND DISCUSSION

A. Metal alloy properties

The wetting properties of the liquid metal both on top and on the trench wall surface were extremely critical for uniformly filling the Si grooves.[4,7] This was demonstrated by a series of experiments with different metal alloys and metal coating of the Si gratings. When the liquid metal did not uniformly wet the Si surface, the metal was unequally distributed over the grooves, filling only some of them. According to the Young-Dupré equation,[11] good wetting (i.e., a contact angle of few degrees) of a liquid metal on a solid substrate can be observed if the adhesion energy is close to the cohesion energy of the liquid. This condition is fulfilled for liquid metals on solid metals regardless of the miscibility between the liquid and the solid because the interfacial bond is metallic.[11] The wetting behavior of the Si template with respect to the liquid Au-Sn alloy was realized by a conformal coating of the Si grating with a metal film. In the reported experiments, we used Ir films deposited by ALD. The wetting properties of the Au-Sn alloy on the Si grating were studied in a previous publication.[7] The Au-Sn alloy (80 wt. % Au–20 wt. % Sn) has a eutectic transition at the temperature of 280 °C. This means that the solid metal foil contains the typical lamellar microstructure of the eutectic alloy, and the grain size for Au-Sn is usually a few hundreds of nanometers or even smaller. The solid–liquid transition occurs at the eutectic temperature, ensuring a fast and sharp phase change at the melting temperature. The strategy to obtain metal casting with eutectic alloys was to apply the pressure during the solid–liquid transition in order to force the liquid metal to flow into the Si grooves and to reduce the flow on the grating top surface.[7] The overall process time was about 30 min, including heating and cooling. An example of this approach is reported in a previous publication.[7]

For the Pb-In alloy, a wetting layer can be created during the thermal process of hot embossing without preliminary ALD coating. This property is due to the presence of In in the compound and because In is a good dopant of Si that forms a chemically stable bonding on the Si surface. The Si grating is dipped in a water diluted HF solution (10 wt. %) for 10 min immediately prior to the hot embossing. The phase diagram of the Pb-In alloy with a composition of 95 wt. % Pb and 5 wt. % In indicated the *solidus* line at 292 °C and the *liquidus* line at 314 °C.[12] With a sufficiently slow heating (10 °C/min) and a long process time (600 s under pressure in the temperature range of 290–330 °C) in the hot-embossing system, the separation of the In-rich phase, according to the phase diagram,[13] with respect to the Pb-rich phase can be observed. Figure 2(a) shows the In-rich nanoparticles formed on the Si surface. The liquid Pb-rich

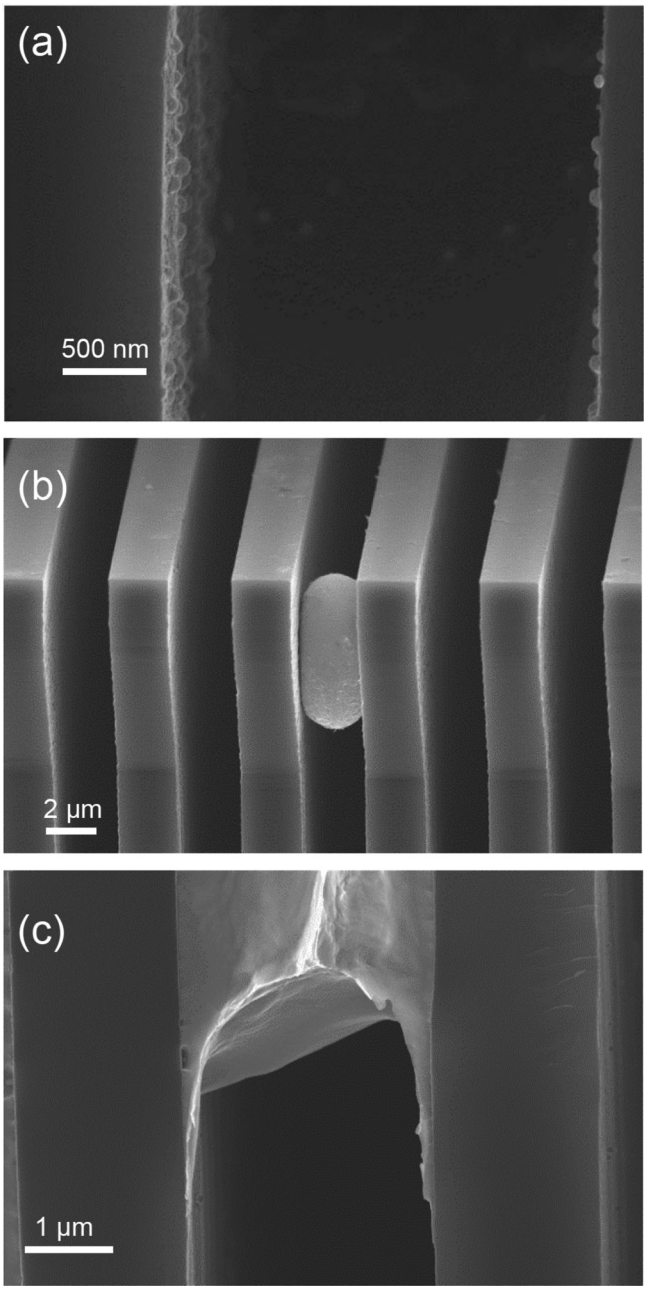

FIG. 2. Pb-In alloy can be separated during melting by slow heating (10 °C/min). The micrographs are high magnification SEM cross-sections of grating trenches where: (a) the In-rich nanoparticles are formed on the HF-cleaned Si surface; (b) the liquid Pb does not wet Si as indicated by the contact angle (>90°); and (c) the liquid Pb-alloy flows on the segregated In coating, which serves as a wetting layer for Pb. Therefore, the system can realize a wetting contact without a significant variation in the composition or even depletion of the alloy. The grating has a pitch of 4.8 μm and was realized by Bosch etch.

compound does not wet Si as indicated by the contact angle (>90°) in Fig. 2(b). However, if the liquid Pb-alloy flows on the In coating, the system can realize a wetting contact, as indicated in Fig. 2(c). Since the alloy has a very small percentage of In (5 wt. %), the In segregation at the Si surface at the beginning of the melting does not significantly affect the final solid composition of the alloy. These results indicated that a sufficiently slow heating and a long process time are the parameters in play to optimize the metal filling without the requirements of any additional ALD wetting layer.

An example of the optimized process is reported in Fig. 3. Slow heating is realized with a temperature gradient between the top and the bottom plate of the hot embossing tool, and the used temperature ramps are shown in Fig. 3(a). The higher temperature of the bottom plate with respect to the top plate promotes the melting of the metal foil from the surface in contact with the Si grating. Figure 3(b) shows the Si grating filled with the Pb-In alloy, the Si grating was realized by MacEtch, the pitch is 6 μm, and the trench depth is 60 μm. The metal casting was realized by applying a pressure of 5 MPa for 600 s.

For the ternary Pb-Sn-Ag alloy, the realization of small pitch gratings is affected by the presence of large micrograins in the foil. During the heating, when the temperature of the process approaches the *solidus* curve in the phase diagram, a liquid containing solid microparticles is formed. Once the *liquidus* curve is reached, the full melting of the metal alloy is realized. The main difference with the eutectic (Au-Sn) system is that the melting is realized in a range of temperatures instead of a single temperature. If the metal is squeezed by hot embossing during the phase between *solidus* and *liquidus*, the solid microparticles can damage the Si template depending on the relative size. An example of this effect is reported in Fig. 4. The metal foil was the Pb-Sn-Ag alloy (92.5 wt. % Pb–5 wt. % Sn–2.5 wt. % Ag, liquidus point 296 °C, solidus 287 °C), and the foil was embossed by applying a pressure of 5 MPa in the temperature range of 285–330 °C for 500 s. The microparticles have sizes in the range of few micrometers, and they are probably Ag segregations since Ag is the metal with the higher melting temperature. Some microparticles were squeezed inside the Si grating with a pitch of 4.8 μm during hot embossing, and they deformed the grating lines, indicating that this kind of metal alloy is not suitable for the realization of grating with the trench size being smaller than 3 μm.

The phase diagram of the metal alloy is used to determine the melting temperature range for the hot embossing experiments. For noneutectic compounds, the microstructure of the metal foil can be extremely relevant for the realization of the metal gratings by metal casting in Si templates.

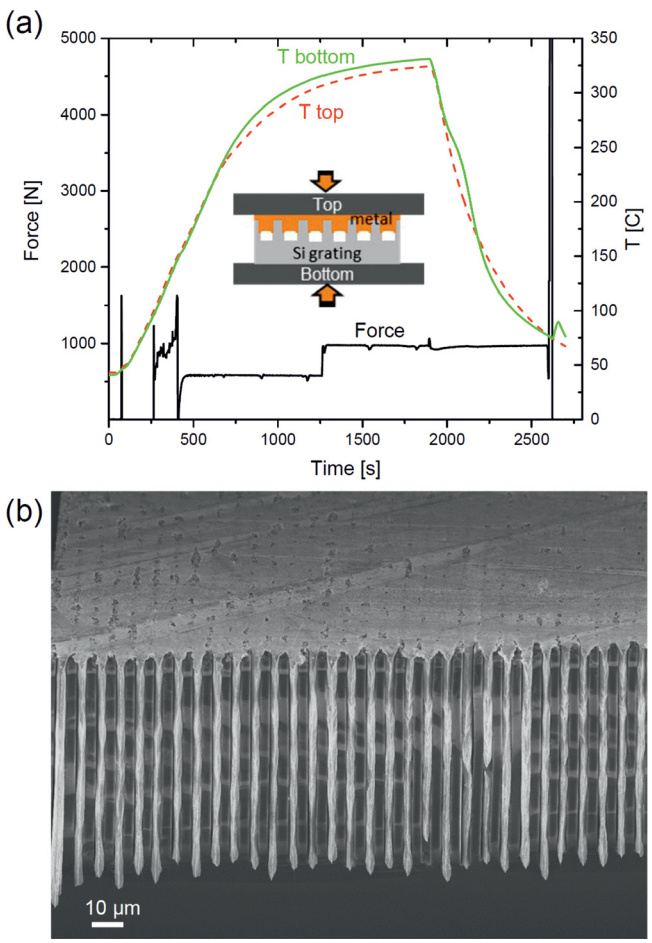

FIG. 3. (Color online) (a) Plot of the hot plate temperature, the bottom plate is in contact with the Si template, the top one with the metal foil as indicated in the inset, the applied force is also reported, and the pressure is about 5 MPa; (b) Pb-In casted grating, the grating area was 20 × 20 mm^2, the pitch is 6 μm, the depth is 60 μm, and the grating was realized by MacEtch.

B. Thermal stress

The metals and Si have different thermal expansion coefficients (Au-Sn:[13] 16 × 10^{-6}/°C; Pb: 28 × 10^{-6}/°C; Si: 3 × 10^{-6}/°C). During cooling, the volume shrinkage of the casted metal lines can be easily observed in the large pitch gratings of Au-Sn (pitch 20 μm) and Pb-In (pitch 4.8 μm) reported in Fig. 5.

The stress released at the interface with Si can cause wafer bowing and cracking. In particular, the brittle nature of crystalline Si with respect to polycrystalline metals leads to the Si fracture.[14] The stress release causes the cracking of

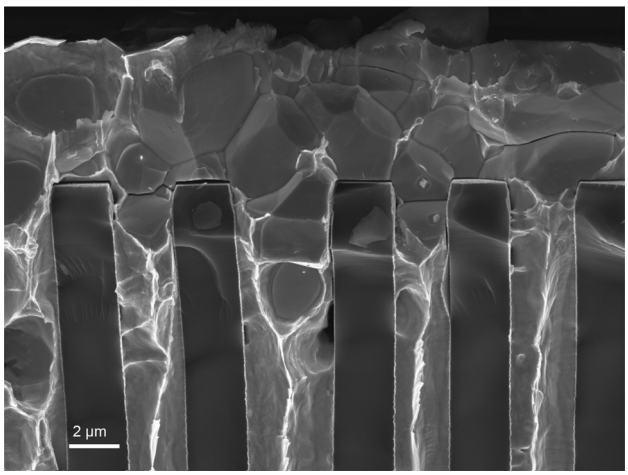

FIG. 4. Pb-Sn-Ag alloy (92.5 wt. % Pb–5 wt. % Sn–2.5 wt. % Ag) casted in the Si grating with a pitch size of 4.8 μm realized by Bosch etch and conformally coated with 30 nm Ir. The hot embossing pressure was 5 MPa at a maximum temperature of 330 °C.

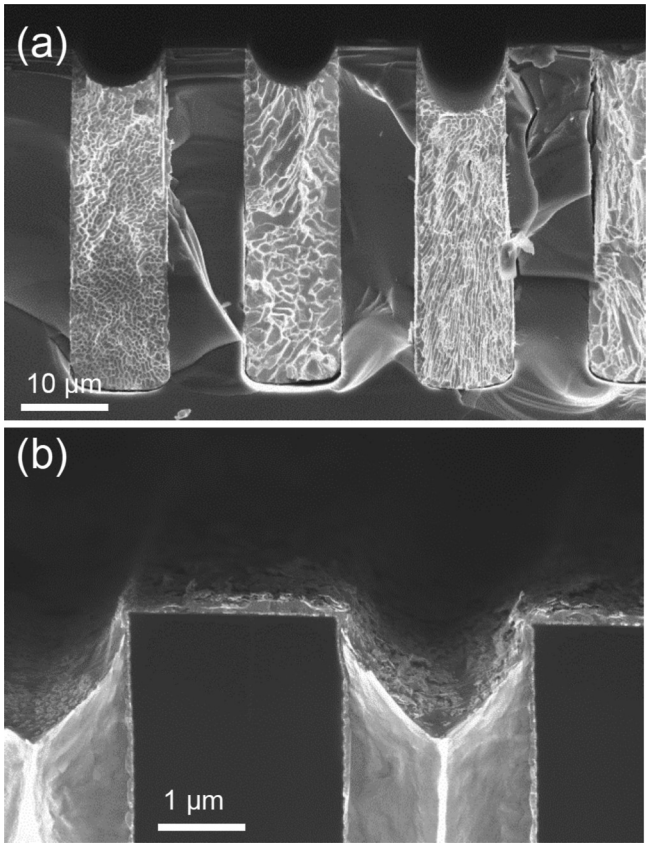

FIG. 5. Au-Sn (a) casted grating with a pitch size of 20 μm; Pb-In (b) casted grating with a pitch size of 4.8 μm. In both gratings, the large grooves are formed on top of the metal lines because of the metal shrinkage during the cooling.

the substrate when the metal is very stiff, which is the case for the Au-Sn alloy [young modulus 68 GPa (Ref. 13)]. This is shown in Fig. 6, the Si grating is cracked along the (111) and (110) planes, and a part of the grating is pulled off with a visible tilt. The pulling off is visible for several millimeters in an optical microscope (not reported) by inspecting the grating surface immediately after the casting process, and so, the cracks are not caused by cleaving of the substrates for the SEM cross-section preparation. The cracks are regularly present with a period of few hundreds of micrometers, as shown in Fig. 6(c). As a consequence, the Si cracking affects the grating performance in the x-ray interferometry. In order to prevent the Si cracking, we performed a very slow cooling step in order to relax the thermal stress. The cooling rate is reported in Fig. 6(a), the fast cooling (black continuous line) produced cracks and the piling up are reported in Figs. 6(b) and 6(c), while the slow cooling (red dotted line) led to intact Si [Figs. 6(d) and 6(e)]. With slow cooling, the stress was released and only produced metal delamination in some lines [Figs. 6(d) and 6(e)]. Delamination does not significantly affect the x-ray performance of the grating since there are no distortions to the surrounding grating lines. Effectively, such a metal delamination has the same effect of local linewidth change for this particular line.

Since the Pb-rich alloys are less stiff (Pb young modulus: 16 GPa), the Si cracking is not observed in this case.

C. High aspect ratio structures

The pressure of the in-printing process is a relevant parameter to ensure the complete filling of the cavities. The process is realized in vacuum (chamber pressure in the range of 100–500 Pa) to avoid the presence of air bubbles inside the grating lines. However, some cavities are formed inside the metal lamellae because of irregularities in the metal foils or metal shrinkage in the cooling phase. Figure 7 shows a comparison of Pb-In casting realized with embossing pressures of 0.4 MPa [Fig. 7(a)] and 1.5 MPa [Fig. 7(b)] into Si grating with a pitch size of 4.8 μm.

High pressure is definitely required to realize metal casting in high aspect ratio gratings, by which the liquid metal is predominantly pushed into the grooves until the voids are filled and the foil volume is completely displaced. This seems to be valid for eutectic, binary, and ternary metals, independent of their different melting behavior. The achieved aspect ratio for all metals is about 50:1. Some examples are reported

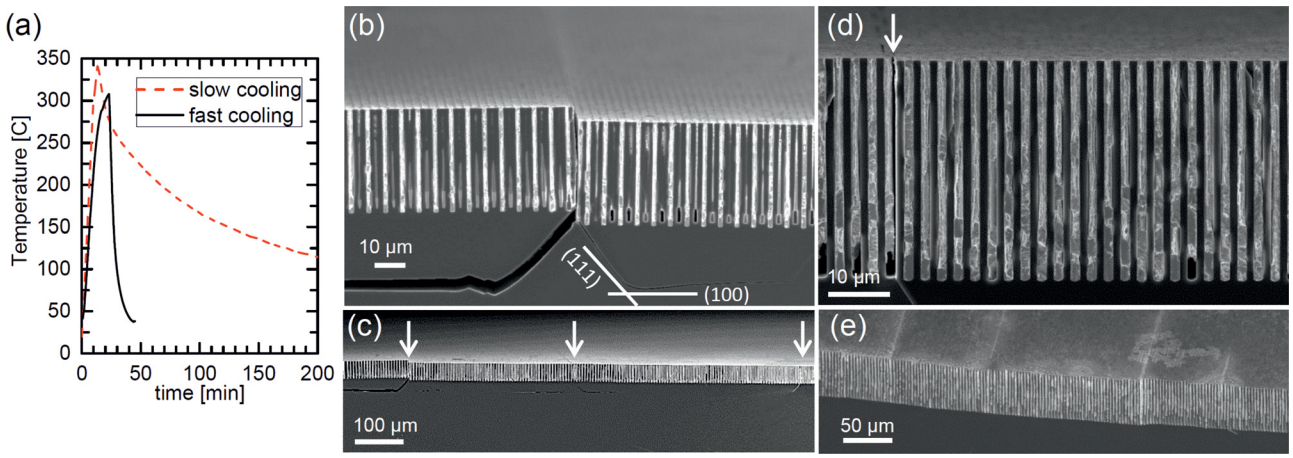

FIG. 6. (Color online) Temperature (a) vs time used for fast and slow cooling experiments. Au-Sn casted grating (b)–(c) obtained with a fast cooling rate. The direction of the Si planes (111) and (110) is plotted as a reference in (b); the arrows in (c) indicate the cracking of the Si substrate along the (111) and (100) directions and grating pulling off due to the release of the thermal stress. Au-Sn casted grating (d) and (e) obtained with the slow cooling rate, the arrow points to delamination, and the low magnification image (e) shows no cracks in Si but only delamination.

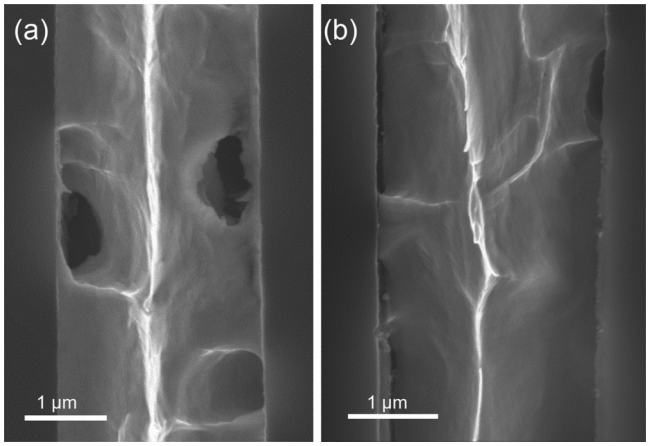

FIG. 7. Pb-In casting realized with embossing pressures of (a) 0.4 MPa and (b) 1.5 MPa into the Si grating with a pitch size of 4.8 μm.

in Figs. 8. Figure 8(a) shows a Si grating with a pitch of 1 μm and a trench depth of 30 μm realized by the Bosch process, coated with the Ir layer by ALD and casted with Pb-In at a pressure of 5 MPa. In this case, the ALD process was performed to ensure the best uniformity of the wetting layer, which is a structure with a very high aspect ratio and a very small pitch (1 μm). Due to the high aspect ratio, the Si lines deformed by bending on one side, and the applied pressure

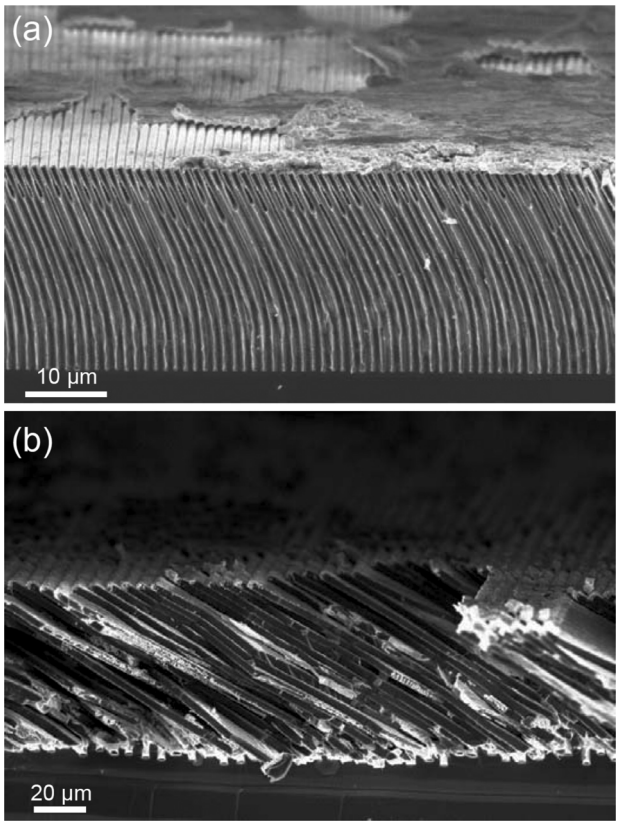

FIG. 8. (a) Grating with a pitch of 1 μm and a trench depth of 30 μm realized by the Bosch process and coated with the Ir layer by ALD, and the casting was realized with Pb-In at a pressure of 5 MPa; (b) Grating with a pitch of 6 μm—a height of 140 μm—realized by MacEtch and casted with Pb-In at 5 MPa. Both gratings have an aspect ratio of 50:1, indicating the limit for applied pressure on high aspect ratio Si lamellae.

was not supported without deformation of the grating. Figure 8(b) reports the same effect for a grating with a pitch of 6 μm and a height of 140 μm realized by MacEtch and casted with Pb-In at 5 MPa. In both cases, a good metal filling was achieved, as the metal can be seen all the way down to the bottom of the Si grooves. The two examples have the same aspect ratio of 50:1 with different pitch sizes, indicating that the smaller pitch size does not limit the aspect ratio of the casting. However, since the filling is complete, which can only occur with an intact grating, i.e., with vertical lamellas, the bending is probably caused by a hard contact between the upper stamper and the grating or an increase in the shearing force, while the foil has only a fraction of its initial thickness (Fig. 8 shows that there are residues of <1 μm). The shearing enables a further compression and thus a bending and possibly a squeezing out of the casted material from the trenches. Therefore, by using thicker foils, it is not unlikely that the aspect ratio can be further enhanced.

The issue is also related to the stability of the high aspect ratio Si lamellae, and it can be solved by introducing some stabilizing structures in the grating geometry. Figure 9(a) shows the Si grating with a pitch size of 2.7 μm and a trench depth of 40 μm realized by the Bosch process, and the bridge lines perpendicular to the main grating pattern are indicated by the arrows. The bridge lines play a role in stabilizing the Si lamellas during the hot embossing process against shearing perpendicular to the lamellas. Figure 9(b) reports the 2.7 μm pitch grating filled with Au-Sn by using the embossing pressure of 5 MPa. The method is successfully applied to also realize Pb-In grating, the grating with a pitch size of 1 μm and a height of 30 μm is reported in Figs. 9(c) and 3(d). However, since the bridge lines limit the metal flow in the direction of the grating lines, more empty cavities at the bottom of the grating were observed [Fig. 9(d)] indicating that the uniformity of the metal filling can be affected by the presence of the stabilizing structures.

The main results of casting Au- and Pb-based alloys by hot embossing in Si gratings in comparison to conventional Au electroplating of gratings produced by deep X-ray lithography[3] are summarized in Table I.

For comparison, the attenuation length of Si for X-ray of 20–30 keV is in the range of 1000–3000 μm so that the absorption from the Si substrate (500 μm thick) of the gratings is negligible for this energy range. However, the Si template can be etched away by using an alkaline solution, which could be useful to produce a full metal grating for the applications where the silicon substrate is undesired (low energy X-ray, bendable gratings, etc.).

D. X-ray performance characterization

The use of the gratings in GI experiments will be reported separately. Here, the focus is on the viability of the fabrication and the possible impact of inhomogeneous casting that cannot be detected in SEM characterization. Preliminary characterization of the Au-Sn gratings shows that the alloys behave like expected, with a smaller absorption resulting

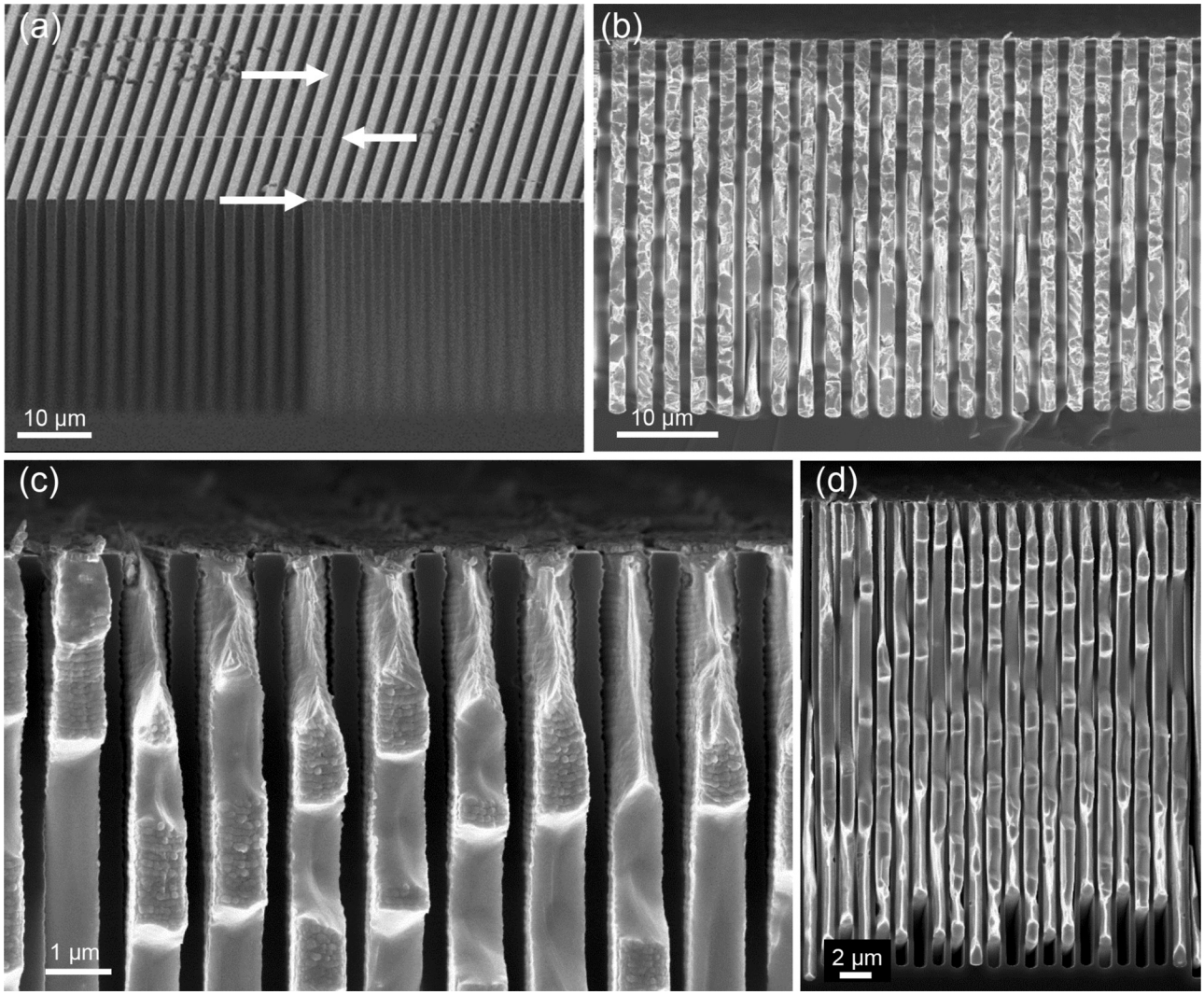

FIG. 9. Si grating (a) with a pitch size of 2.7 μm and a trench depth of 40 μm realized by the Bosch process, and the bridge lines perpendicular to the main grating pattern are indicated by the arrows; grating filled with Au-Sn (b) by using the embossing pressure of 5 MPa; grating with a pitch size of 1 μm and a height of 30 μm and hot embossed with Pb-In (c) and (d) at 5 MPa.

from the composition of the alloy, i.e., 80 wt. % for Au-Sn in comparison to electroplated Au gratings.

Due to the X-ray source characteristics, X-ray grating interferometry systems typically consist of a combination of two[1] (synchrotron-based setups) or three X-ray gratings[16] (laboratory-based systems). In the latter case, the system consists of a source absorbing grating (G0), a phase grating (G1), and an analyzer absorbing grating (G2), and thus, the casted gratings are suitable to be used as absorbing G0 or G2.

In particular, the X-ray performance of Au-Sn casted gratings with a pitch of 4.8 μm (casting thickness 30 μm, grating area $70 \times 70\,\text{mm}^2$) was investigated by a symmetric grating interferometer geometry[16] for a design photon energy of 20 keV in the third Talbot order. The system was built by mounting a set of three gratings on a high precision stage. The total length of the system was 55.8 cm. Initially, the Au-Sn casted grating was used as a G0 grating together with a G1 phase grating made of silicon and a G2 absorbing grating fabricated by Au electroplating. An average X-ray fringe visibility of 14.0%, which is comparable to the values achieved in absorbing gratings fabricated by conventional gold electroplating, was observed. After that, the gratings were exchanged, the Au-Sn casted grating was used as G2, and an average X-ray fringe visibility of 16.4% was obtained. The difference in values is caused by different X-ray filtering properties of the gratings, which suggests that different energy ranges of X-rays are incident on the G1 phase grating, which affects the contrast of interference produced by the gratings. The visibility map (visibility at each x-ray camera pixel) and differential phase contrast and scattering images of the sample consisting of polystyrene microspheres of size 600 μm are shown in Fig. 10. The good quality of the Au-Sn casted grating is observed in the obtained images of the sample.

The same kind of characterization has been performed with the Pb-In grating, and the preliminary results with the Pb-In grating (pitch of 4.8 μm, thickness of 50 μm, and grating size of $20 \times 20\,\text{mm}^2$) as G2 indicate a mean visibility of 12.7% for a design photon energy of 20 keV in the third Talbot order. Further experiments are necessary to optimize the GI system set up.

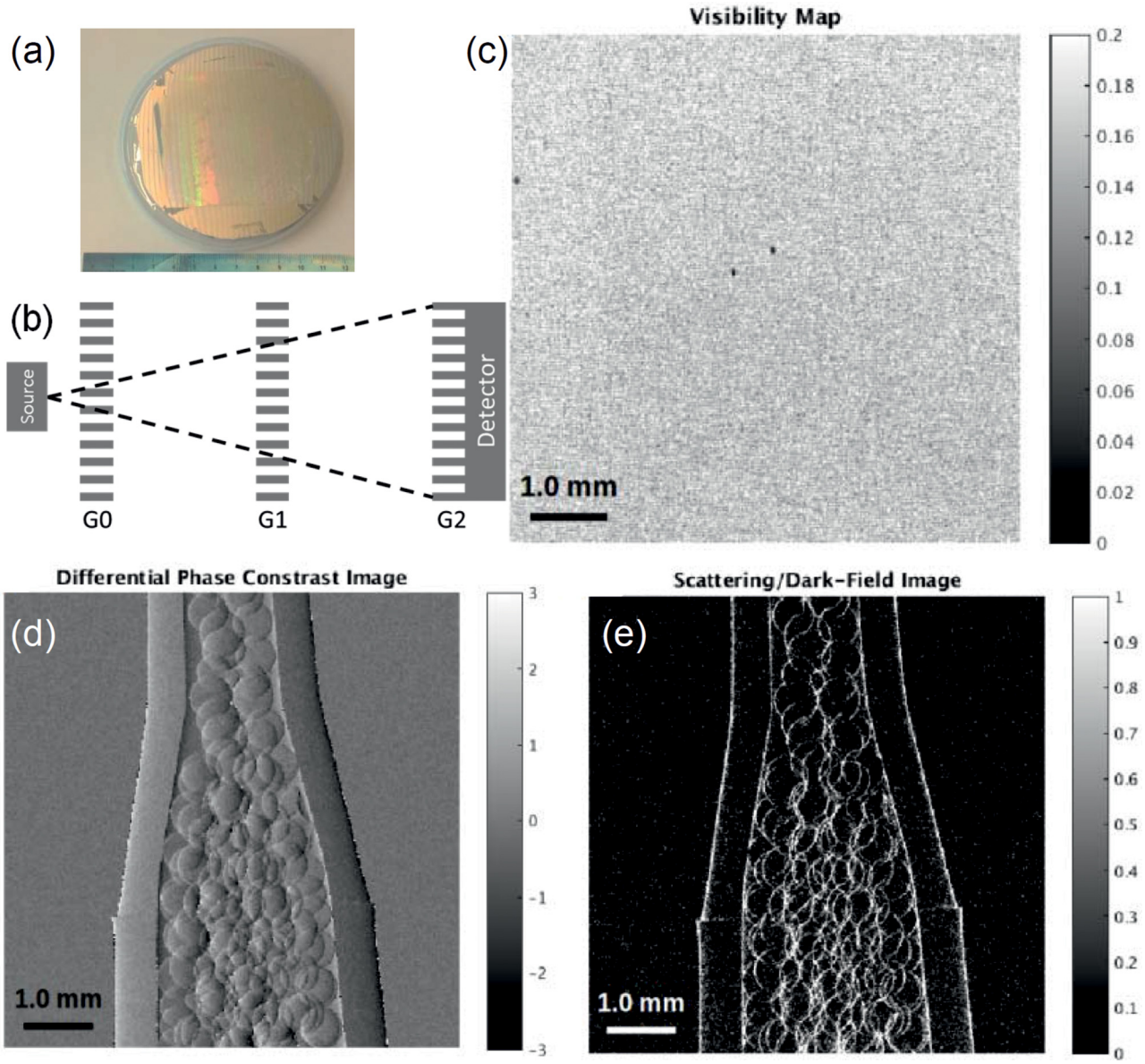

FIG. 10. (Color online) X-ray performance of the Au-Sn casted grating of 4.8 μm period used as a G2 absorbing grating. (a) casted grating (100 mm wafer with a 70 $\times$ 70 mm^2 grating area); schematic (not in scale) of the X-ray interferometer (Ref. 16) (b); X-ray fringe visibility map (c); differential phase contrast (d) and scattering (e) images of 600 μm polystyrene spheres.

IV. SUMMARY AND CONCLUSIONS

High aspect ratio metal microgratings can be fabricated by direct hot embossing of metal foils into Si gratings. The material properties such as the metal wetting on the Si template, the alloy phase diagram, the metal shrinkage during the solidification, and the associated stress release contribute to the uniformity and the quality of the manufacturing. The hot embossing parameters such as the heating/cooling ramp and the applied pressure have to be finely tuned as a function of the used metal alloy and grating aspect ratio. We tested Au-Sn, Pb-In, and Pb-Sn-Ag alloys underlying the different relevant peculiarities. A slow cooling is necessary in order to avoid the Si cracking in Au-Sn casted gratings. This issue is not relevant for Pb-based alloys, with Pb being less stiff than the Au alloy. The Pb-In alloy has a good wettability of the Si surface because of the presence of In that can create a self-wetting layer for the liquid alloy without the necessity of the Ir wetting layer used for the Au-Sn alloy. The Pb-Sn-Ag alloy forms a liquid-phase containing microsized solid particles that damage the Si grating lines during the hot embossing, and so, it cannot be used for grating line sizes smaller than 3 μm.

The casted gratings were tested using an X-ray GI setup in order to compare their performance with respect to Au electroplated gratings. A visibility in the range of 15% at 20 keV was obtained using Au-Sn casted gratings. The metal gratings are key components for X-ray phase sensitive GI systems. The new method has relevant advantages, such as being a low cost technique, fast, and easily scalable to large area fabrication. The presented low cost and high yield fabrication process has a direct impact on the commercialization of X-ray GI for medical diagnostics and nondestructive testing.

ACKNOWLEDGMENTS

This work was partially funded by the ERC-2012-STG 310005-PhaseX Grant, ERC-PoC-2016 727246-MAGIC Grant. The authors would like to thank the following people for their valuable collaboration and contributions: K. Vogelsang, S. Stutz, V. Guzenko, and C. David from PSI-LMN; M. Kagias, C. Arboleda, and Z. Wang from PSI-TOMCAT.

[1]T. Weitkamp, A. Diaz, C. David, F. Pfeiffer, M. Stampanoni, P. Cloetens, and E. Ziegler, Opt. Express **13**, 6296 (2005).
[2]C. David, J. Bruder, T. Rohbeck, C. Grünzweig, C. Kottler, A. Diaz, O. Bunk, and F. Pfeiffer, Microelectron. Eng. **84**, 1172 (2007).
[3]J. Mohr, T. Grund, D. Kunka, J. Kenntner, J. Leuthold, J. Meiser, J. Schulz, and M. Walter, AIP Conf. Proc. **1466**, 41 (2012).
[4]Y. Lei, L. Xin, L. Ji, G. Jinchuan, and N. Hanben, J. Micromech. Microeng. **26**, 065011 (2016).
[5]Y. Lei, D. Yang, L. Ji, Z. Zhigang, L. Xin, G. Jinchuan, and N. Hanben, J. Micromech. Microeng. **24**, 015007 (2014).
[6]L. Yaohu, D. Yang, L. Ji, H. Jianheng, Z. Zhigang, L. Xin, G. Jinchuan, and N. Hanben, Appl. Phys. Express **6**, 117301 (2013).
[7]L. Romano, J. Vila-Comamala, M. Kagias, K. Vogelsang, H. Schift, M. Stampanoni, and K. Jefimovs, Microelectron. Eng. **176**, 6 (2017).
[8]K. Jefimovs, L. Romano, J. Vila-Comamala, M. E. Kagias, Z. Wang, L. Wang, C. Dais, H. Solak, and M. Stampanoni, Proc. SPIE **10146**, 101460L (2017).
[9]L. Romano, J. Vila-Comamala, K. Jefimovs, and M. Stampanoni, Microelectron. Eng. **177**, 59 (2017).
[10]L. Romano, M. Kagias, K. Jefimovs, and M. Stampanoni, RSC Adv. **6**, 16025 (2016).
[11]N. Eustathopoulos, Metals **5**, 350 (2015).
[12]J. P. Nabot and I. Ansara, *Binary Alloy Phase Diagrams*, edited by T. B. Massalski (ASM International, 1990), Vol. 3, p. 2669.
[13]T. Zhou, T. Bobal, M. Oud, and J. Songliang, "Au/Sn solder alloy and its applications in electronics packaging," http://www.ametek-ecp.com/-/media/ametek-ecp/files/cwtechnicalpapers/coining_english_gold_tin_paper.pdf.
[14]R. F. Cook, J. Mater. Sci. **41**, 841 (2006).
[15]"X-ray attenuation length," http://henke.lbl.gov/optical_constants/atten2.html.
[16]T. Donath *et al.*, J. Appl. Phys. **106**, 054703 (2009).